J|A|C|S
ARTICLES
Published on Web 06/20/2002

Nitride Formation by Thermolysis of a Kinetically Stable Niobium Dinitrogen Complex

Michael D. Fryzuk,* Christopher M. Kozak, Michael R. Bowdridge, Brian O. Patrick,† and Steven J. Rettig†,‡

Contribution from the Department of Chemistry, University of British Columbia, 2036 Main Mall, Vancouver, British Columbia, V6T 1Z1, Canada

Received February 21, 2002

Abstract: The reduction of $[P_2N_2]NbCl$ (where $[P_2N_2] = PhP(CH_2SiMe_2NSiMe_2CH_2)_2PPh$) with KC_8 under a dinitrogen atmosphere generates the paramagnetic dinuclear dinitrogen complex $([P_2N_2]Nb)_2(\mu\text{-}N_2)$ (**2**). Complex **2** has been characterized crystallographically and by EPR spectroscopy. Variable-temperature magnetic susceptibility measurements indicate that **2** displays antiferromagnetic coupling between two Nb(IV) (d^1) centers. A density functional theory calculation on the model complex $[(PH_3)_2(NH_2)_2Nb]_2(\mu\text{-}N_2)$ was performed. Thermolysis of $([P_2N_2]Nb)_2(\mu\text{-}N_2)$ in toluene generates the paramagnetic bridging nitride species where one N atom of the dinitrogen ligand inserts into the macrocycle backbone to form $[P_2N_2]$-$Nb(\mu\text{-}N)Nb[PN_3]$ (**3**) (where $[PN_3] = PhPMe(CHSiMe_2NSiMe_2CH_2P(Ph)CH_2SiMe_2NSiMe_2N)$). Complex **3** has been characterized in the solid state as well as by variable-temperature magnetic susceptibility measurements. The reaction of $([P_2N_2]Nb)_2(\mu\text{-}N_2)$ with phenylacetylene displaces the dinitrogen fragment to generate a paramagnetic η^2-alkyne complex, $[P_2N_2]Nb(\eta^2\text{-}HCCPh)$ (**4**).

Introduction

The literature concerning the synthesis and characterization of dinitrogen complexes is experiencing a resurgence. This has been fueled by a number of separate events that include the X-ray characterization of the active site of a nitrogenase enzyme,[1] the observation of new bonding modes for the dinitrogen ligand in coordination chemistry,[2,3] the reports of new transformations of coordinated dinitrogen that involve reaction with H_2 and silanes,[4] and the formation of nitrides from coordinated N_2.[5−9] Taken together these results suggest that this area is undergoing a renaissance.[10]

The cleavage of coordinated dinitrogen to generate metal nitride derivatives is considered to be a fundamental process in nitrogen fixation both industrially and biologically.[3,11−13] The recent discovery that bulky molybdenum(III) tris(amide) complexes cleave N_2 to form Mo(VI) nitrides was the first of a series of important studies of nitride formation from coordinated dinitrogen.[5−7,14,15] Many of these systems involve the formation of a dinuclear dinitrogen complex as an observed intermediate.[6,8] Irrespective of observable intermediates, a total of six electrons must be formally added to the dinitrogen unit, and so far this has been best accomplished by using two metal centers.

In this paper we present our attempts to design a system that can activate dinitrogen and furthermore induce N−N bond cleavage to generate a nitride complex. Our success with the formation of the side-on bound dinuclear zirconium dinitrogen complex,[4] $([P_2N_2]Zr)_2(\mu\text{-}\eta^2\text{:}\eta^2\text{-}N_2)$ (where $[P_2N_2] = PhP(CH_2$-$SiMe_2NSiMe_2CH_2)_2PPh$), provided a starting point since incorporation of the same macrocyclic ancillary ligand system onto a group 5 metal (i.e., V, Nb, or Ta) would formally provide one extra electron per metal over that found for the aforementioned zirconium analogue. If one assumes that the formation of $([P_2N_2]Zr)_2(\mu\text{-}\eta^2\text{:}\eta^2\text{-}N_2)$ corresponds to a formal addition of 4 electrons to neutral N_2, then the availability of an additional two electrons per dinuclear group 5 complex would provide the necessary six electrons required for cleavage of dinitrogen.

We recently reported the synthesis of niobium(III) complexes of the $[P_2N_2]$ ligand system.[16,17] In this work, we examine the preparation and characterization of a dinuclear dinitrogen complex of niobium, its reactivity with protons and alkynes, and its thermolysis to form a dinuclear nitride species.

* Corresponding author. E-mail: fryzuk@chem.ubc.ca.
† UBC X-ray Structural Chemistry Laboratory.
‡ Deceased October 27, 1998.

(1) Kim, J.; Rees, D. C. *Nature* **1992**, *360*, 563.
(2) Fryzuk, M. D.; Johnson, S. A.; Patrick, B. O.; Albinati, A.; Mason, S. A.; Koetzle, T. K. *J. Am. Chem. Soc.* **2001**, *123*, 3960.
(3) Fryzuk, M. D.; Johnson, S. A. *Coord. Chem. Rev.* **2000**, *200−202*, 379.
(4) Fryzuk, M. D.; Love, J. B.; Rettig, S. J.; Young, V. G. *Science* **1997**, *275*, 1445.
(5) Laplaza, C. E.; Cummins, C. C. *Science* **1995**, *268*, 861.
(6) Laplaza, C. E.; Johnson, M. J. A.; Peters, J. C.; Odom, A. L.; Kim, E.; Cummins, C. C. *J. Am. Chem. Soc.* **1996**, *118*, 8623.
(7) Laplaza, C. E.; Johnson, A. R.; Cummins, C. C. *J. Am. Chem. Soc.* **1996**, *118*, 709.
(8) Caselli, A.; Solari, E.; Scopelliti, R.; Floriani, C.; Re, N.; Rizzoli, C.; Chiesi-Villa, A. *J. Am. Chem. Soc.* **2000**, *122*, 3652.
(9) Clentsmith, G. K. B.; Bates, V. M. E.; Hitchcock, P. B.; Cloke, F. G. N. *J. Am. Chem. Soc.* **1999**, *121*, 10444.
(10) Leigh, G. J. *Chem. Br.* **2001**, *May*, 23.
(11) Gambarotta, S. *J. Organomet. Chem.* **1995**, *500*, 117.
(12) Hidai, M.; Mizobe, Y. *Chem. Rev.* **1995**, *95*, 1115.
(13) Leigh, G. J. *Acc. Chem. Res.* **1992**, *25*, 177.
(14) Cummins, C. C. *Chem. Commun.* **1998**, 1777.
(15) Peters, J. C.; Cherry, J. F.; Thomas, J. C.; Baraldo, L.; Mindiola, D. J.; Davis, W. M.; Cummins, C. C. *J. Am. Chem. Soc.* **1999**, *121*, 10053.
(16) Fryzuk, M. D.; Kozak, C. M.; Bowdridge, M. R.; Jin, W.; Tung, D.; Patrick, B. O.; Rettig, S. J. *Organometallics* **2001**, *20*, 3752.
(17) Fryzuk, M. D.; Kozak, C. M.; Mehrkhodavandi, P.; Morello, L.; Patrick, B. O.; Rettig, S. J. *J. Am. Chem. Soc.* **2002**, *124*, 516.

Results and Discussion

Synthesis and Structure of the Niobium Dinitrogen Compound, $([P_2N_2]Nb)_2(\mu\text{-}N_2)$ (2). Our continued interest in the synthesis of dinitrogen compounds and the availability of the Nb(III) starting complex $[P_2N_2]NbCl$ (**1**)[16] prompted us to examine its ability to bind N_2 under reducing conditions. Within group 5, there are a number of dinitrogen complexes of vanadium and tantalum that have been reported;[2,18−30] however, those of niobium continue to be rare.[8,31−34] Reduction of $[P_2N_2]$-NbCl (**1**) by KC_8 in toluene under 1 atm of N_2 for 48 h allows isolation of a dark brown paramagnetic solid in 85% yield that has been characterized as $([P_2N_2]Nb)_2(\mu\text{-}N_2)$ (**2**). Varying the reaction conditions by changing the solvent to THF, increasing the pressure of N_2 to 4 atm, or performing the reaction at temperatures from −78 to +65 °C did not appear to affect the yield. Reaction of 1 equiv of $PbCl_2$ with a brown toluene solution of $([P_2N_2]Nb)_2(\mu\text{-}N_2)$ overnight caused the appearance of a deep green solution and a gray precipitate of metallic lead. Filtration followed by removal of solvent allowed isolation of a red solid that was spectroscopically characterized as the starting niobium(III) chloride, $[P_2N_2]NbCl$ (**1**) (Scheme 1).

The ^1H NMR spectrum of dinitrogen complex **2** shows only broadened resonances from which no structural information could be determined. However, mass spectrometry indicates a *m*/*z* peak of 1278, which correlates to the dinuclear complex **2** in Scheme 1. The presence of a dinitrogen ligand was confirmed by protonation of **2** by $Me_3N{\cdot}HCl$ and the successful detection of hydrazine (62%). Dark brown, X-ray quality crystals were obtained from slow evaporation of a toluene solution. The solid-state molecular structure is shown in Figure 1, with crystallographic data listed in Table 1. The X-ray data indicate the dinitrogen ligand is bound in an end-on fashion bridging the two niobium centers. The coordination geometry of each niobium center is a distorted trigonal bipyramid, with the three nitrogen ligands (two from the macrocycle and one from the bridging N_2) occupying the equatorial plane (sum of the equatorial angles is 360.0°); the phosphorus donors lie in slightly pinched back apical positions giving P(1)−Nb(1)−P(2) and P(3)−Nb(2)−P(4) angles of 161.07(5)° and 162.35(5)°, respectively, which are consistent with those observed in other early transition metal complexes of $[P_2N_2]$.[16,35−37] The two $[P_2N_2]$-Nb ends of **2** are staggered with respect to each other about the axis defined by the Nb(1)−N(5)−N(6)−Nb(2) unit; the P(1)−Nb(1)−Nb(2)−P(4) dihedral angle is 59.6°. The P−Nb−P and N−Nb−N angles displayed in the macrocycle are not unusual with respect to those previously observed in pentacoordinate

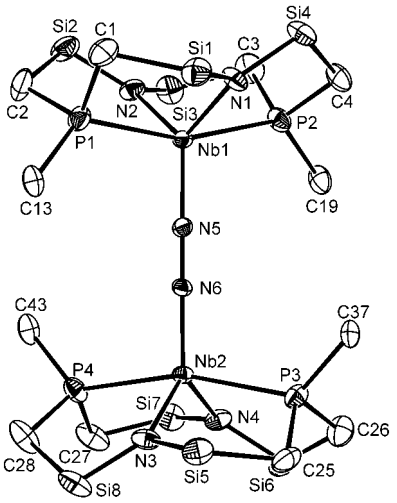

Figure 1. Molecular structure (ORTEP) of $([P_2N_2]Nb)_2(\mu\text{-}N_2)$ (**2**). Ellipsoids are drawn at the 30% probability level, silyl methyl groups are omitted for clarity, and only ipso carbons of phenyl rings are shown. Selected bond lengths (Å), angles (deg), and dihedral angles (deg): N(5)−N(6), 1.272(5); Nb(1)−N(5), 1.853(4); Nb(2)−N(6), 1.850(4); Nb(1)−P(1), 2.5729(14); Nb(1)−P(2), 2.5799(14); Nb(1)−N(1), 2.171(4); Nb(1)−N(2), 2.157(4); Nb(2)−P(3), 2.5709(15); Nb(2)−P(4), 2.5720(15); Nb(2)−N(3), 2.156(4); Nb(2)−N(4), 2.149(4); Nb(1)−N(5)−N(6), 179.5(3); Nb(2)−N(6)−N(5), 179.1(3); P(1)−Nb(1)−P(2), 161.07(5); N(1)−Nb(1)−N(2), 116.1(2); P(3)−Nb(2)−P(4), 162.35(5); N(3)−Nb(2)−N(4), 114.9(2); N(1)−Nb(1)−N(5), 123.8(2); N(2)−Nb(1)−N(5), 120.1(2); N(3)−Nb(2)−N(6), 121.7(2); N(4)−Nb(2)−N(6), 123.4(2); N(1)−Nb(1)−P(1), 85.77(11); N(1)−Nb(1)−P(2), 83.57(11); N(2)−Nb(1)−P(1), 84.35(11); N(2)−Nb(1)−P(2), 86.36(12); N(3)−Nb(2)−P(3), 86.47(12); N(3)−Nb-(2)−P(4), 84.26(12); N(4)−Nb(2)−P(3), 84.09(13); N(4)−Nb(2)−P(4), 86.24(13); P(1)−Nb(1)−Nb(2)−P(4), 59.6.

Scheme 1

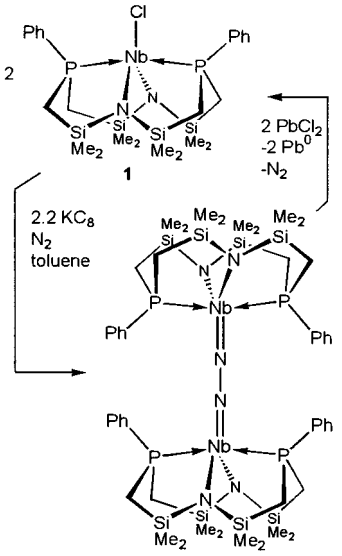

(18) Song, J.-I.; Berno, P.; Gambarotta, S. *J. Am. Chem. Soc.* **1994**, *116*, 6927.
(19) Berno, P.; Hao, S. K.; Minhas, R.; Gambarotta, S. *J. Am. Chem. Soc.* **1994**, *116*, 7417.
(20) Buijink, J. K. F.; Meetsma, A.; Teuben, J. H. *Organometallics* **1993**, *12*, 2004.
(21) Ferguson, R.; Solari, E.; Floriani, C.; Osella, D.; Ravera, M.; Re, N.; Chiesi-Villa, A.; Rizzoli, C. *J. Am. Chem. Soc.* **1997**, *119*, 10104.
(22) Ferguson, R.; Solari, E.; Floriani, C.; Chiesivilla, A.; Rizzoli, C. *Angew. Chem., Int. Ed. Engl.* **1993**, *32*, 396.
(23) Rehder, D.; Woitha, C.; Priebsch, W.; Gailus, H. *J. Chem. Soc., Chem. Commun.* **1992**, 364.
(24) Woitha, C.; Rehder, D. *Angew. Chem., Int. Ed. Engl.* **1990**, *29*, 1438.
(25) Leigh, G. J.; Prietoalcon, R.; Sanders, J. R. *J. Chem. Soc., Chem. Commun.* **1991**, 921.
(26) Turner, H. W.; Fellman, J. D.; Rocklage, S. M.; Schrock, R. R.; Churchill, M. R.; Wasserman, H. J. *J. Am. Chem. Soc.* **1980**, *102*, 7809.
(27) Schrock, R. R.; Wesolek, M.; Liu, A. H.; Wallace, K. C.; Dewan, J. C. *Inorg. Chem.* **1988**, *27*, 2050.
(28) Rocklage, S. M.; Turner, H. W.; Fellman, J. D.; Schrock, R. R. *Organometallics* **1982**, *1*, 703.
(29) Churchill, M. R.; Wasserman, H. J. *Inorg. Chem.* **1981**, *20*, 2899.
(30) Churchill, M. R.; Wasserman, H. J. *Inorg. Chem.* **1982**, *21*, 218.
(31) Berno, P.; Gambarotta, S. *Organometallics* **1995**, *14*, 2159.
(32) Zanotti-Gerosa, A.; Solari, E.; Giannini, L.; Floriani, C.; Chiesi-Villa, A.; Rizzoli, C. *J. Am. Chem. Soc.* **1998**, *120*, 437.
(33) Dilworth, J. R.; Henderson, R. A.; Hills, A.; Hughes, D. L.; MacDonald, C.; Stephens, A. N.; Walton, D. R. M. *J. Chem. Soc., Dalton Trans.* **1990**, 1077.
(34) Rocklage, S. M.; Schrock, R. R. *J. Am. Chem. Soc.* **1982**, *104*, 3077.
(35) Fryzuk, M. D.; Johnson, S. A.; Rettig, S. J. *Organometallics* **1999**, *18*, 4059.
(36) Fryzuk, M. D.; Johnson, S. A.; Rettig, S. J. *Organometallics* **2000**, *19*, 3931.
(37) Fryzuk, M. D.; Love, J. B.; Rettig, S. J. *Organometallics* **1998**, *17*, 846−853.

Table 1. Crystallographic Data[a]

	2	3	4
formula	$C_{48}H_{84}N_6Nb_2P_4Si_8$	$C_{48}H_{84}N_6Nb_2P_4Si_8$	$C_{32}H_{48}N_2NbP_2Si_4$
FW	1279.62	1279.62	727.94
color, habit	brown, prism	blue, block	red, irregular chip
crystal size, mm^3	0.35 × 0.40 × 0.45	0.35 × 0.25 × 0.25	0.40 × 0.20 × 0.10
crystal system	monoclinic	monoclinic	orthorhombic
space group	$P2_1/n$ (no. 14)	$P2_1/c$ (no. 14)	$Pna2_1$ (no. 33)
a, Å	16.1151(11)	14.527(1)	15.8295(6)
b, Å	15.887(2)	13.4604(9)	12.5210(4)
c, Å	26.0621(7)	33.633(3)	19.466(1)
α, deg	90	90	90
β, deg	92.8130(4)	99.360(4)	90
γ, deg	90	90	90
V, Å^3	6664.6(7)	6489.1(8)	3858.3(5)
Z	4	4	4
T, °C	−93 ± 1	−100 ± 1	−75 ± 1
ρ_{calc}, g/cm^3	1.275	1.310	1.253
μ(Mo Kα), cm^{-1}	6.18	6.35	5.42
$R(F, I \geq 3\sigma(I))$	0.073	0.061	0.027
$R_w(F, I \geq 3\sigma(I))$	0.069	0.141	0.031
$R(F^2$, all data)	0.114	0.101	0.048
$R_w(F^2$, all data)	0.124	0.1537	0.070
gof	2.59	1.01	0.83

[a] Rigaku/ADSC CCD diffractometer, $R = \sum||F_o^2| - |F_c^2||/\sum|F_o^2|$; $R_w = (\sum w(|F_o^2| - |F_c^2|)^2/\sum w|F_o^2|^2)^{1/2}$.

Table 2. N−N Bond Lengths in Niobium Dinitrogen Complexes

compd	N–N bond length (Å)	ref
$[(Et_2NCS_2)_3Nb]_2(\mu\text{-}N_2)$	1.252(16)	33
$[(Cy_2N)_3Nb]_2(\mu\text{-}N_2)$	1.34(1)	31
$[\{p\text{-}Bu^t\text{-calix}[4]\text{-}(O)_4Nb\}_2(\mu\text{-}N_2)]Na_2$	1.390(17)	8
$([NPN]NbCl)_2(\mu\text{-}N_2)$	1.237(4)	2
$([P_2N_2]Nb)_2(\mu\text{-}N_2)$	1.272(5)	this work

niobium chloride and alkyl complexes.[16] The niobium atoms themselves are joined by a linear end-on bridging N_2 unit with Nb(1)−N(5)−N(6) and Nb(2)−N(6)−N(5) angles of 179.5(3)° and 179.1(3)°, respectively. The N−N bond length of 1.272(5) Å is slightly longer than that observed in diazobenzene (1.255 Å) but shorter than that observed in hydrazine (1.46 Å). A comparison of N−N bond lengths in previously reported niobium dinitrogen complexes appears in Table 2.

If one assumes that the N−N bond length in **2** more closely approximates a N−N double bond of a diazenido type linkage, an N_2^{2-} unit, then each niobium center should correspond to a formal oxidation state of +3 (the $[P_2N_2]$ ligand is assigned a −2 charge). However, as will be discussed below, the EPR data and variable-temperature magnetic studies are more consistent with a formalism in which both metal centers are Nb(IV).

The EPR spectrum of **2** displays a decet of triplets centered at $g = 1.975$ (Figure 2). The 30 line pattern results from coupling of a single unpaired electron to a $I = {}^9/_2$ ^{93}Nb nucleus ($a(^{93}Nb) = 108.2$ G) and two $I = {}^1/_2$ ^{31}P nuclei ($a(^{31}P) = 22.9$ G). The solid-state magnetic susceptibility (χ_m) of the dinitrogen compound, **2**, was measured from 2 to 300 K with a SQUID magnetometer. The plot of magnetic susceptibility per dimer vs temperature shows a broad maximum at 120 K, indicating the presence of antiferromagnetic exchange. The magnetic moment decreases upon cooling the sample to 2 K, consistent with the sample approaching a singlet ground state. The room-temperature magnetic moment of 2.9 μ_B per mole of dimer appears high if one assumes the presence of two d^1 Nb(IV) centers in dinitrogen complex **2**. However, large spin−orbit coupling characteristic of second- and third-row transition metals in addition to the presence of temperature-independent para-

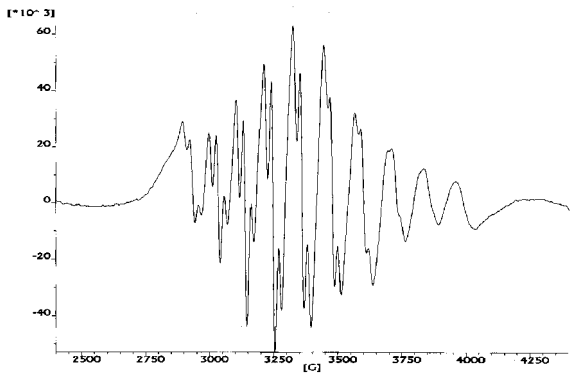

Figure 2. EPR spectrum of $([P_2N_2]Nb)_2(\mu\text{-}N_2)$ (**2**) in toluene, $g = 1.975$, $a(^{93}Nb) = 108.2$ G, $a(^{31}P) = 22.9$ G at 300 K.

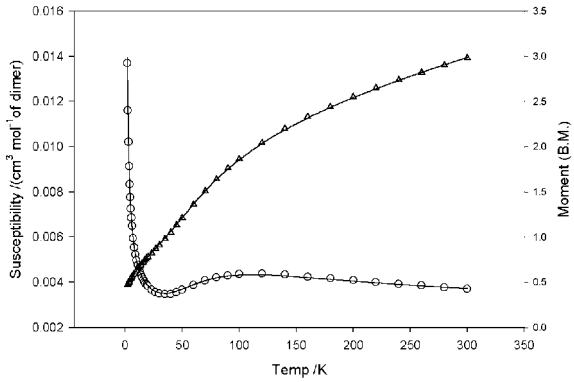

Figure 3. Magnetic susceptibility (○) and moment (△) versus temperature plot per mole of $([P_2N_2]Nb)_2(\mu\text{-}N_2)$ (**2**). The Bleaney−Bowers model was employed to generate the lines with $J = -67.5$ cm^{-1}, $g = 1.975$, TIP = 0.0027 cm^3 mol^{-1}, and $P = 0.061$ ($F = 0.0077$).

magnetism (TIP) likely account for the observed moment. The data can be modeled (Figure 3) by using the Bleaney−Bowers equation, assuming the interaction between the two spin centers can be described by the Heisenberg spin Hamiltonian $H = -2JS_1 \cdot S_2$, considering a pair of exchange-coupled centers where $S_1 = S_2 = {}^1/_2$. To account for the presence of a small amount of paramagnetic impurity the expression was combined with the Curie law term,

$$\chi_{para} = \frac{N_A g^2 \mu_B{}^2 S(S+1)}{3kT}$$

according to

$$\chi_m = [1 - P]\chi_{Nb} + P\chi_{para}$$

where P represents the fraction of paramagnetic $S = 1$ impurity.

The presence of temperature-independent paramagnetism (TIP) was also included in the model. The resulting analysis of the collected data yielded $g = 1.975$, $J = -67.5$ cm^{-1}, $P = 0.061$, and TIP = 0.0027 cm^3 mol^{-1}. These results indicate a significant amount of antiferromagnetic coupling between the two $S = {}^1/_2$ spin centers through the N−N bridge and despite the comparatively short N−N bond the coordinated N_2 ligand can be formally considered a hydrazido, N_2^{4-}, moiety. Antiferromagnetic coupling via N−N bonds has been observed previously for related dinuclear vanadium dinitrogen complexes, but the magnitude of the coupling is very small or negligible.[38]

Table 3. Selected Bond Lengths, Bond Angles ,and Dihedral Angles for the ab Initio DFT Geometry Optimization of the Model Complex $[(H_3P)_2(H_2N)_2Nb]_2(\mu\text{-}N_2)$ (**2A**); Total Energy = −479.309 Ha

atom	atom	distance (Å)	atom	atom	distance (Å)
$N_{dinitrogen}$	$N_{dinitrogen}$	1.255	Nb	P	2.636
Nb	$N_{dinitrogen}$	1.925	Nb	N_{amide}	2.065

atom	atom	atom	angle (deg)	atom	atom	atom	angle (deg)
Nb(1)	N(5)	N(6)	179.99	P(1)	Nb(1)	P(1)	160.00
N(1)	Nb(1)	N(2)	113.00	N(1)	Nb(1)	P(1)	84.18
N(5)	Nb(1)	P(1)	100.00	N(1)	Nb(1)	P(2)	84.82

atom	atom	atom	atom	dihedral angle (deg)
P(1)	Nb(1)	Nb(2)	P(3)	96.8
P(1)	Nb(1)	N(5)	N(6)	58.9

Density Functional Theory Analysis of the Bonding in $([P_2N_2]Nb)_2(\mu\text{-}N_2)$. Geometry optimizations were performed by using density functional theory. To simplify the calculations the model complex $[(H_3P)_2(H_2N)_2Nb]_2(\mu\text{-}N_2)$ (**2A**) was studied with restrictions placed on the $N_{dinitrogen}-Nb-N_{amide}-H$ dihedral angles. These restrictions were intended to mimic the rigid geometry imposed by the $[P_2N_2]$ ligand, which prevents the amido donors from freely rotating. The geometry of model complex **2A** was optimized (with the exception of the previously stated constraints) with use of the Gaussian 98 program[39] and the hybrid functional B3LYP method.[40] The basis functions and effective core potentials (ECP) used were those in the LANL2DZ basis set[41] but with additional d-polarization functions added to P atoms with the exponent of the d-functions set at 0.37. This level of theory has been used previously in the study of dinitrogen complexes.[2,3]

Selected optimized bond lengths, bond angles, and dihedral angles for the model complex **2A** are shown in Table 3. The numbering scheme used is the same as for the structure of complex **2** shown in Figure 1. The general features of the optimized geometry of this model complex are in good agreement with the structure of complex **2** except that the model complex attains a geometry where the $[P_2N_2]$ ligands exhibit a P(1)−Nb(1)−Nb(2)−P(3) torsion angle of 96.8° about the Nb−N_2−Nb axis (Figure 4). Also, the model displays slightly elongated Nb−P and Nb−$N_{dinitrogen}$ bonds. This inconsistency between model complex **2A** and the structure of complex **2** may be attributed to crystal packing effects that may be strongly influenced by the presence of phenyl groups on the phosphine donor atoms.

The experimental evidence for dinitrogen to bind end-on to transition metals is overwhelming,[3,11,12] although more examples of the side-on bridging mode are becoming known. The predominance of the end-on binding mode has been rationalized

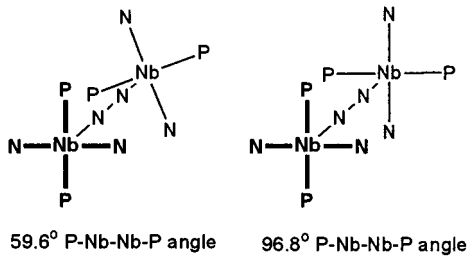

Figure 4. Depiction of ligand geometries for the crystallographically observed 59.6° and the calculated 96.8° P−Nb−Nb−P torsion angles in **2**.

qualitatively for two ML_4 fragments with a single N_2 unit.[42] The ML_4 fragments possess three available d orbitals (d_{xy}, d_{xz}, and d_{yz}) that point between the M−L and N_2 ligands while the remaining d_{z2} and $d_{x^2-y^2}$ orbitals are utilized in σ-bonding with the ligands. In the end-on bridging mode, the symmetrical interaction with the π*-orbitals of the N_2 molecule generates two molecular orbitals in the M−(μ-N_2)−M fragment with π-symmetry, which, if occupied, would be bonding for the metal−nitrogen interaction, but antibonding with respect to the N_2 unit itself. For the analogous side-on bonding mode, as observed in $([P_2N_2]Zr)_2(\mu\text{-}\eta^2\text{:}\eta^2\text{-}N_2)$, one generates two bonding molecular orbitals: one of π-symmetry and the other of δ-symmetry. These too are both bonding with respect to the metal−nitrogen interaction but antibonding for the N_2 fragment. However, the δ-molecular orbital is less stabilized than the respective π-molecular orbital and as such the end-on bonding mode that favors π-interaction is preferred on energetic grounds.

The existence of an end-on bonded dinitrogen fragment in **2** rather than the side-on bonding mode exhibited by $([P_2N_2]Zr)_2(\mu\text{-}\eta^2\text{:}\eta^2\text{-}N_2)$ can be explained by an examination of the occupied molecular orbitals. As has been shown by previously reported ab initio and semiempirical studies of bridging dinitrogen compounds,[38,43,44] the metal−nitrogen bonding molecular orbitals are present in the nearly degenerate HOMO-2 and HOMO-3 orbitals. The HOMO and HOMO-1 are the entirely metal centered orbitals of d_δ symmetry, as expected. For a Nb(IV) (d^1) center, the HOMO is singly occupied. In $([P_2N_2]Zr)_2(\mu\text{-}\eta^2\text{:}\eta^2\text{-}N_2)$ this orbital is vacant and can therefore participate in a δ-bonding interaction with the π* orbital of the N_2 fragment. Because the δ orbitals have no contribution from the bridging N_2 ligand, it is surprising that any significant antiferromagnetic coupling is observed between the two formally d^1 metal centers. A π(N−N) bonding combination and a π(M−N) antibonding combination of orbitals describe the LUMO. Normally this precludes any orbital overlap, but by nature of the crystallographically imposed "twist" there appears to be a possibility for M−N orbital overlap resulting in a potential pathway for antiferromagnetic coupling to occur.

Thermolysis of $([P_2N_2]Nb)_2(\mu\text{-}N_2)$ (2). It has been shown that a molybdenum(III) tris(amide) readily coordinates dinitrogen and subsequently undergoes thermolysis to generate a molybdenum nitride.[5−7] Bearing in mind that the two Nb(IV) centers in our $([P_2N_2]Nb)_2(\mu\text{-}N_2)$ complex can in theory each act as a one-electron reductant, the further reduction of the hydrazido N_2^{4-} ligand to nitrido N^{3-} seems plausible. Heating

(38) Ferguson, R.; Solari, E.; Floriani, C.; Osella, D.; Ravera, M.; Re, N.; ChiesiVilla, N.; Rizzoli, C. *J. Am. Chem. Soc.* **1997**, *119*, 10104.
(39) Frisch, M. J.; Trucks, G. W.; Schlegel, H. B.; Scuseria, G. E.; Robb, M. A.; Cheeseman, J. R.; Zakrzewski, V. G.; Montgomery, J. A.; Stratmann, R. E.; Burant, J. C.; Dapprich, S.; Millam, J. M.; Daniels, A. D.; Kudin, K. N.; Strain, M. C.; Farkas, O.; Tomasi, J.; Petersson, V. A.; Ayala, P. Y.; Cui, Q.; Morokuma, K.; Malick, D. K.; Rabuck, A. D.; Raghavachari, K.; Foresman, J. B.; Cioslowski, J.; Ortiz, J. V.; Stefanov, B. B.; Liu, G.; Liashenko, A.; Piskorz, P.; Komaromi, I.; Gomperts, R.; Martin, R. L.; Fox, D. J.; Keith, T.; Al-Laham, M. A.; Peng, C. Y.; Nanayakkara, A.; Gonzalez, C.; Challacombe, M.; Gill, P. M. W.; Johnson, B. G.; Chen, W.; Wong, M. W.; Andres, J. L.; Head-Gordon, M.; Repogle, E. S.; Pople, J. A. *Gaussian 98*, Revision A.7; Gaussian, Inc.: Pittsburgh PA, 1998.
(40) Becke, A. D. *J. Chem. Phys.* **1993**, *98*, 5648.
(41) Hay, P. J.; Wadt, W. R. *J. Chem. Phys.* **1985**, *82*, 270.
(42) Fryzuk, M. D.; Haddad, T. S.; Mylvaganam, M.; McConville, D. H.; Rettig, S. J. *J. Am. Chem. Soc.* **1993**, *115*, 2782.
(43) Re, N.; Rosi, M.; Sgamellotti, A.; Floriani, C.; Solari, E. *Inorg. Chem.* **1994**, *33*, 4390.
(44) Powell, C. B.; Hall, M. B. *Inorg. Chem.* **1984**, *23*, 4619.

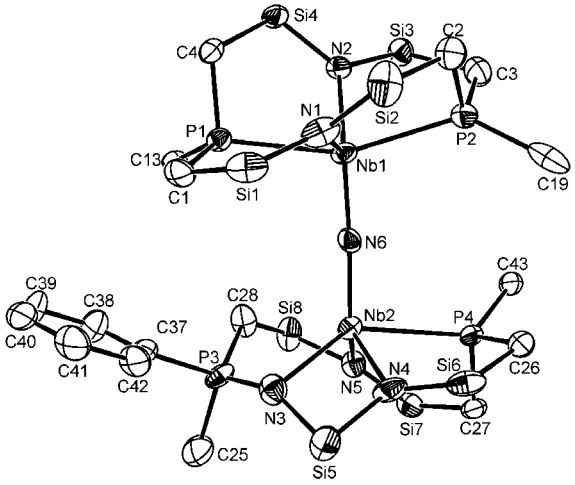

Figure 5. Molecular structure of $[P_2N_2]Nb(\mu\text{-}N)Nb[PN_3]$, **3**. Ellipsoids are drawn at the 50% probability level, silyl methyl groups are omitted for clarity, and only ipso carbons of phenyl groups on P(1), P(2), and P(4) are shown. Selected bond lengths (Å), angles (deg), and dihedral angles (deg): Nb(1)−N(1), 2.119(5); Nb(1)−N(2), 2.146(4); Nb(1)−P(1), 2.5761(13); Nb(1)−P(2), 2.564(2); Nb(1)−N(6), 1.913(4); Nb(2)−N(3), 2.271(5); Nb(2)−N(4), 2.135(4); Nb(2)−N(5), 2.130(4); Nb(2)−N(6), 1.866(4); Nb(2)−P(4), 2.6089(13); Nb(2)···P(3), 2.9169(19); P(3)−N(3), 1.554(6); P(3)−C(28), 1.672(7); P(3)−C(25), 1.844(8); P(1)−Nb(1)−P(2), 156.23(6); N(1)−Nb(1)−N(2), 110.39(17); P(1)−Nb(1)−N(6), 99.14(12); P(2)−Nb(1)−N(6), 104.43(12); N(1)−Nb(1)−N(6), 118.58(18); N(2)−Nb(1)−N(6), 129.96(17); Nb(1)−N(6)−Nb(2), 168.8(2); N(4)−Nb(2)−N(5), 115.57(18); N(3)−Nb(2)−N(4), 66.6(2); N(3)−Nb(2)−N(5), 104.04(19); N(3)−Nb(2)−N(6), 116.5(2); N(4)−Nb(2)−N(6), 115.43(19); P(4)−Nb(2)−N(6), 95.76(12); N(5)−Nb(2)−N(6), 123.81(18).

a degassed brown toluene solution of $([P_2N_2]Nb)_2(\mu\text{-}N_2)$ to 110 °C in a sealed ampule for 12 h causes the formation of a paramagnetic blue-green product. Mass spectrometry shows the absence of a *m*/*z* peak at 1278 but instead displays an intense peak at 639 corresponding to a $[P_2N_2]NbN$ fragment. This peak is absent in the mass spectrum of **2**. The structure of the thermolysis product **3** was determined by X-ray crystallography and is shown in Figure 5 along with selected bond lengths and angles. Crystallographic data are given in Table 1. What becomes apparent is that the N−N bond has been cleaved, but rather than generating either a monomeric terminal nitride or dimeric bridging species, a single nitride bridging two niobium nuclei is observed. The second nitrogen atom of the N_2 fragment has instead inserted into the backbone of one of the $[P_2N_2]$ macrocycles to form the bimetallic bridging nitride complex $[P_2N_2]Nb(\mu\text{-}N)Nb[PN_3]$ (**3**) (where $[PN_3]$ = PhPMe($CHSiMe_2NSiMe_2CH_2P(Ph)CH_2SiMe_2NSiMe_2N$)) (eq 1).

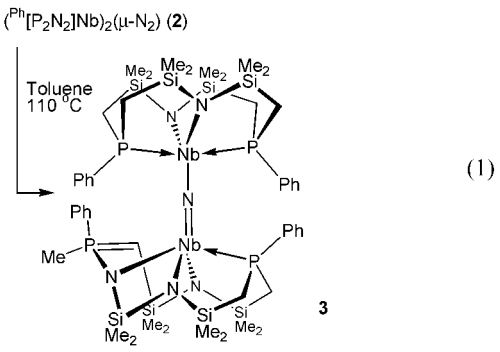

(1)

The structure of **3** was found to be disordered but was refined without invoking any restrictions on atom designation. The

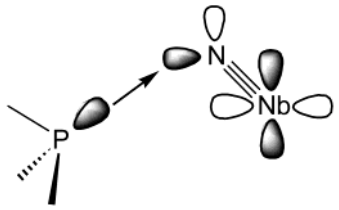

Figure 6. Proposed orbital interactions in phosphorus−nitride coupling.

Nb(2)−N(3) distance of 2.271(5) Å is longer than the Nb(2)−N(4) and Nb(2)−N(5) bond lengths of 2.135(4) and 2.130(4) Å, respectively. This elongated Nb−N bond may be a product of constraints within the macrocycle. The P(3)−C(28) bond length of 1.672(7) Å is shorter than the distances observed between P(4)−C(26), 1.812(6) Å, and P(4)−C(27), 1.830(5) Å, and suggests a P=C double bond. The P(3)−N(3) distance of 1.554(6) Å is shorter than expected for a typical P−N single bond and may possess some double bond character. Another possibility is that N(3) and C(28) may be disordered over two sites. However, the long interatomic distance between C(28) and Nb(2) of 2.537 Å suggests the absence of a bonding interaction. The paramagnetic nature of **3** prevents the observation of any interpretable NMR spectrum. Nitride **3** is also EPR silent, suggesting the existence of zero-field splitting. This is consistent with the variable-temperature magnetic susceptibility data (see below).

Several groups have studied the mechanism of N−N bond cleavage in early transition metal complexes.[6,8,9] The cleavage of the dinitrogen ligand in **2** may be compared to the N−N bond cleavage exhibited by a niobium calix[4]arene complex where it has been suggested that reduction of niobium by sodium generates a "biradical system", effectively creating two Nb(IV), d^1 centers.[8] Cleavage proceeds via a side-on bound dinitrogen intermediate stabilized by a resulting Nb−Nb bond that undergoes thermally induced intramolecular transfer from the metal−metal bond to the N−N bond. In our system, the initial reduction step is not required as both niobium centers are already at the required Nb(IV) oxidation state. The insertion of one of the resulting nitrido groups into the macrocycle backbone is less straightforward, likely proceeding via nitride formation followed by reaction of a phosphine donor with an electrophilic nitride (Scheme 2).[45] Nitride coupling reactions have been proposed to occur via an unsymmetrical transition state geometry in which the lone pair of one nitride interacts with an empty M≡N π^* orbital of another.[46,47] In such a transition state, one nitride acts as a nucleophile at the nitrogen whereas the other acts as an electrophile. In our system, the phosphine lone pair can be envisioned to donate into the M≡N π^* orbital of the nitride (Figure 6). Electron transfer from the nitride into the C−Si bond generates a phosphamethylene and subsequent proton transfer occurs resulting in the formation of an ylide-type fragment.

The thermolysis can be followed by using UV−visible spectroscopy. The dark brown color of the dinitrogen complex in toluene solution is observed to change to blue-green as the solution is heated at 110 °C over time. The UV−visible spectrum shows the diminishment of a peak at 440 nm

(45) Nugent, W. A.; Mayer, J. M. *Metal−Ligand Multiple Bonds*; John Wiley & Sons: Toronto, Canada, 1988.
(46) Ware, D. C.; Taube, H. *Inorg. Chem.* **1991**, *30*, 4605.
(47) Seymore, S. B.; Brown, S. N. *Inorg. Chem.* **2001**, *41*, 462.

Scheme 2

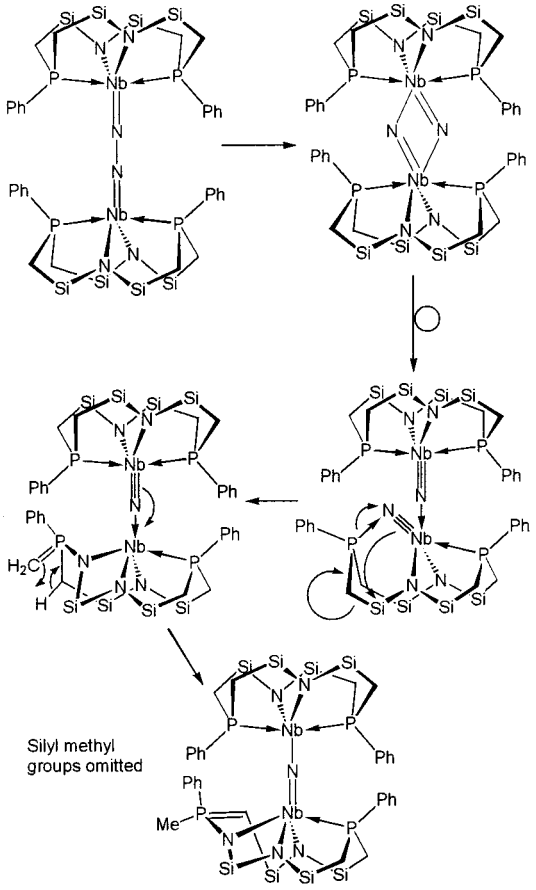

attributable to the starting dinitrogen compound and the growth of an absorption at 652 nm that is ascribed to the nitride complex, **3**. The presence of a single isosbestic point indicates that no stable intermediate product, namely the bridging bis(nitride) species, is formed and that any such intermediates are short-lived.

Magnetic Studies of Nitride (3). The solid-state magnetic susceptibility of complex **3** was studied between 2 and 300 K with a SQUID magnetometer. Unlike complex **2**, the plot of magnetic susceptibility vs temperature does not indicate any antiferromagnetic coupling. The magnetic moment shows a steady decrease as the temperature is lowered from 300 to 20 K. The moment then drops abruptly as the temperature approaches 2 K. These results are consistent with an isolated $S = 1$ spin center possessing a singlet ground state and a thermally populated triplet state.

The magnetic moment of 3.2 at 300 K is higher than expected for two unpaired electrons, however, this may be due to a large TIP. Attempts to model the data by using simple Curie or Curie−Weiss behavior did not provide good fits. As we have observed for previous noncoupled Nb(III) complexes,[16] contributions from zero-field splitting effects in second- and third-row transition metals are significant. The magnetic susceptibility data for **3** were therefore analyzed by using the equation for the zero-field splitting of a $S = 1$ state:

$$\chi_{Nb} = {}^1/_3C\left[\frac{2e^{-x}}{1+2e^{-x}}\right] + {}^2/_3C\left[\frac{(2/x)(1-e^{-x})}{1+2e^{-x}}\right]$$

where $x = D/kT$ and $C = N_A g^2 \mu_B{}^2/kT$. Contributions from the

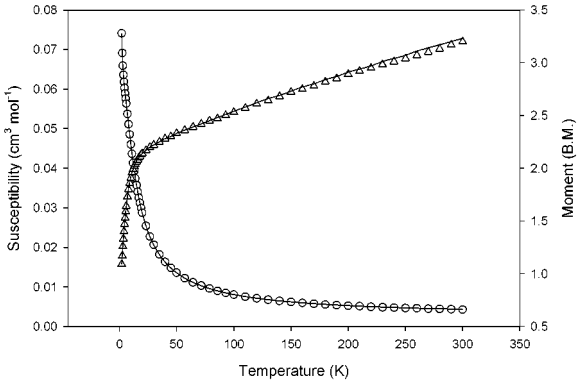

Figure 7. Magnetic susceptibility (○) and moment (△) versus temperature plot for $[P_2N_2]Nb(\mu\text{-}N)Nb[PN_3]$, **3**. The zero field splitting model was employed to generate the lines with $D = 15.05$ cm^{-1}, $g = 1.49$, TIP = 0.0025, and $P = 0.0088$ ($F = 0.007$).

presence of a small amount of paramagnetic impurity were accounted for as in the analysis of **2**, above. Experimental data for **3** are compared with the best fits from theory yielding $D = 15.05$ cm^{-1}, $g = 1.49$, TIP = 0.0025, and $P = 0.0088$ ($F = 0.007$) (Figure 7). The small g value can be rationalized by the large degree of spin−orbit coupling exhibited by Nb. Such observed behavior is consistent with pairs of d^2−d^0 ions rather than pairs of d^1-d^1 ions, suggesting a change in oxidation states of the niobium centers to Nb(III)−Nb(V). This is supported by the crystallographic evidence that indicates a shorter Nb(2)−N(6) bond than Nb(1)−N(6), suggesting Nb(2) has been oxidized to Nb(V) whereas Nb(1) has undergone a reduction to Nb(III).

Reaction of 2 with Phenylacetylene. We have previously reported the unprecedented reactivity of the zirconium dinitrogen complex $([P_2N_2]Zr)_2(\mu\text{-}\eta^2\text{:}\eta^2\text{-}N_2)$ with H_2 and primary silanes where the dinitrogen ligand undergoes N−H and N−Si bond formation, respectively.[4] The reactivity of $([P_2N_2]Nb)_2(\mu\text{-}N_2)$ (**2**) with small molecules was also examined; however, **2** shows no reactivity with H_2 or H_3SiR.

Terminal acetylenes have been observed to induce N−C bond formation at the dinitrogen moiety in $([P_2N_2]Zr)_2(\mu\text{-}\eta^2\text{:}\eta^2\text{-}N_2)$.[48] Although the dinitrogen unit in **2** is bound in the end-on fashion, its susceptibility to protonation suggested that it might be reactive toward terminal acetylenes. Addition of 2 equiv of phenylacetylene to a brown toluene solution of **2** results in an immediate reaction to form a dark red solution. Although the dark red paramagnetic product obtained gives a broadened and shifted ^{1}H NMR spectrum, mass spectrometry shows a *m*/*z* peak corresponding to a $[P_2N_2]Nb(HCCPh)$ fragment. This formulation was confirmed by elemental analysis.

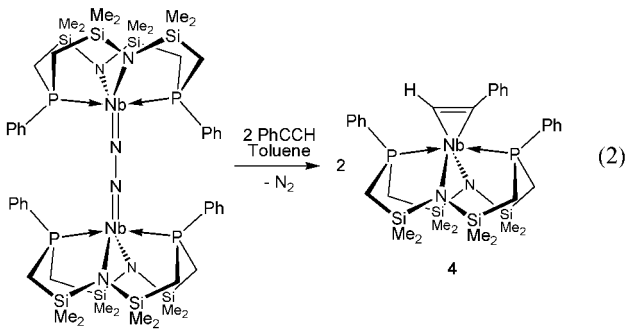

(2)

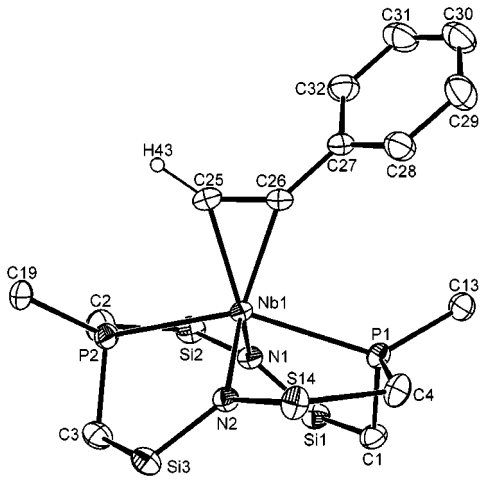

Figure 8. Molecular structure (ORTEP) of $[P_2N_2]Nb(\eta^2\text{-HCCPh})$, **4**. Ellipsoids are drawn at the 30% probability level, silyl methyl groups are omitted for clarity, and only ipso carbons of phenyl rings are shown. Selected bond lengths (Å), angles (deg), and dihedral angles (deg): C(25)−C(26), 1.307(5); Nb(1)−C(25), 2.100(3); Nb(1)−C(26), 2.124(3); Nb(1)−P(1), 2.5756(8); Nb(1)−P(2), 2.5449(8); Nb(1)−N(1), 2.116(2); Nb(1)−N(2), 2.127(2); C(25)−C(26)−C(27), 137.4(3); P(1)−Nb(1)−P(2), 152.04(3); N(1)−Nb(1)−N(2), 110.76(9); P(1)−Nb(1)−N(1), 85.52(6); P(1)−Nb(1)−N(2), 79.20(7); P(2)−Nb(1)−N(1), 79.72(6); P(2)−Nb(1)−N(2), 84.00(7); P(1)−Nb(1)−C(25), 123.67(9); P(1)−Nb(1)−C(26), 87.62(9); P(2)−Nb(1)−C(25), 84.29(9); P(2)−Nb(1)−C(26), 120.34(9); N(1)−Nb(1)−C(25), 118.4(1); N(1)−Nb(1)−C(26), 120.7(1); N(2)−Nb(1)−C(25), 126.2(1); N(2)−Nb(1)−C(26), 125.5(1); P(1)−Nb(1)−C(25)−C(26), 0.6(3); P(2)−Nb(1)−C(26)−C(27), −171.0(5); N(1)−Nb(1)−C(25)−C(26), −104.1(2); N(2)−Nb(1)−C(25)−C(26), 102.6(2).

The displacement of the dinitrogen ligand by phenylacetylene was confirmed by single-crystal X-ray molecular structure determination. The structure of $[P_2N_2]Nb(\eta^2\text{-HCCPh})$ is shown in Figure 8 and crystallographic data are given in Table 1. The reaction of phenylacetylene with **2** therefore appears to involve the displacement of the bound dinitrogen moiety as dinitrogen gas, and the binding of phenylacetylene to produce an η^2-acetylide $[P_2N_2]Nb(\eta^2\text{-HCCPh})$, **4** (eq 2). The niobium atom resides in a distorted trigonal bipyramidal geometry if the alkyne ligand is considered to occupy one coordination site. The two amides and the alkyne occupy the equatorial positions while the phosphine groups occupy slightly pinched back apical positions. Interestingly, the coordination of the alkyne group is coplanar to the apical phosphine donors; a brief description of the bonding interactions in **4** is discussed below.

The Nb−P and Nb−N bond lengths are fully comparable to those observed in **2**, above. The N−Nb−N and P−Nb−P angles of 110.76(9)° and 152.04(3)°, respectively, in **4** are, however, significantly smaller than the corresponding angles observed in complex **2**. Steric effects imposed upon the macrocycle by the phenylacetylene unit likely cause this decrease in bond angles. The alkyne ligand in **4** is best described as being a four-electron donor where both π-systems are involved in the bonding to the transition metal. The system can therefore be described as containing a formally Nb(II) (d^3) center that adopts a resonance form where the metal is in an oxidized Nb(IV) (d^1) state. An examination of the relevant bond lengths confirms this description, thus the system formally possesses a niobium(IV), d^1 center. The Nb(1)−C(25) and Nb(1)−C(26) bond lengths of 2.100(3) and 2.124(3) Å, respectively, are in the range expected for a Nb−C single bond and the C(25)−C(26) bond length of 1.307(5) Å corresponds to a bond order of 2.2.[49] Also, the C(25)−C(26)−C(27) angle shows a considerable distortion from the free ligand. These lengths and angles agree with those previously reported for systems described as containing four-electron-donating alkyne fragments and are consistent with the complex being viewed as a niobacyclopropene fragment with the metal in a formally +4 oxidation state.[50,51]

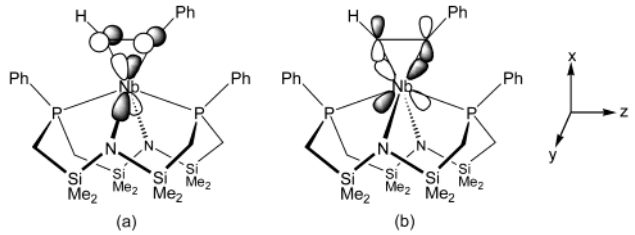

Figure 9. (a) Overlap of alkyne $\pi_\perp$ MO with metal d_{xy} orbital shared by σ-bond formation with $[P_2N_2]$ amide donors. (b) Interaction of the filled d_{xz} orbital with the vacant $\pi_{||}$* orbital.

Solution magnetic susceptibility measurement by Evans method gives a magnetic moment of 1.4 μ_B consistent with one unpaired electron. Alkyne complex **4** is EPR active and, like dinitrogen complex **2**, displays a decet of triplets. The 30 line spectrum is centered at $g = 1.985$ and results from coupling of the unpaired electron to the $I = {}^9/_2$ ^{93}Nb nucleus ($a(^{93}\text{Nb}) = 108.4$ G) and two $I = {}^1/_2$ ^{31}P nuclei ($a(^{31}\text{P}) = 21.6$ G). No coupling to the acetylene proton was observed.

The coordination of the alkyne ligand is coplanar to the phosphine donors. Assuming the alkyne ligand occupies one coordination site, the niobium center can be considered to possess a mildly distorted trigonal-bipyramidal geometry, thus, the frontier orbital description is similar to that presented for dinitrogen complex **2**, above. The phosphine donors are considered to lie along the *z*-axis while the amide donors occupy the *xy*-plane. Thus, the vacant d_{xy} and d_{z^2} orbitals are stabilized by σ-bonding with the amide and phosphine donors, respectively. The bonding of the alkyne ligand is accomplished by three molecular orbitals of π-symmetry, $\pi_\perp$, $\pi_{||}$, and $\pi_{||}$*. The filled d_{xz} orbital is of appropriate symmetry to interact with the vacant $\pi_{||}$* orbital. The filled $\pi_{||}$ orbital is therefore well suited to interact with the empty $d_{x^2-y^2}$ orbital to form a σ-bond. Last, the filled $\pi_\perp$ orbital of the alkyne is of appropriate symmetry to donate into the d_{xy} orbital, which is also experiencing σ-bond interaction with the amide donors (Figure 9). The d_{yz} orbital undergoes no interaction with the alkyne; as shown in the DFT calculations for dinitrogen complex **2** above the d_{yz} orbital is the singly occupied HOMO.

Conclusion

The goal of this work was to examine the formation of nitrides by investigation of the coordination chemistry of $[P_2N_2]$ with a group 5 metal. Reduction of $[P_2N_2]$NbCl under dinitrogen was expected to lead to the formation of a niobium−nitride complex on the basis of a total of six electrons added. Instead, the isolation of the kinetically stable dinuclear dinitrogen complex $([P_2N_2]Nb)_2(\mu\text{-}N_2)$, **2**, was observed. The variable-temperature

(48) Fryzuk, M. D.; Love, J. B.; Morello, L. Unpublished results.

(49) Curtis, M. D.; Real, J.; Kwon, D. *Organometallics* **1989**, *8*, 1644.
(50) Etienne, M.; Mathieu, R.; Donnadieu, B. *J. Am. Chem. Soc.* **1997**, *119*, 3218.
(51) Templeton, J. L. *Adv. Organomet. Chem.* **1999**, *29*, 1.

magnetic properties of complex **2** were examined and indicate the existence of antiferromagnetic exchange between two Nb(IV) (d^1) centers. However, thermolysis of **2** does result in the formation of nitrides, albeit complicated by ligand rearrangement. The isolation of $[P_2N_2]Nb(\mu\text{-}N)Nb[PN_3]$, **3**, not only illustrates that nitrides can be formed by using the combination of group 5 elements and the $[P_2N_2]$ ligand set, but that the nitrides can be functionalized; in this case, N−P and N−Si bond formation is observed although the overall process is stoichiometric. The overall transformation of **2** to **3** is also significant in that attack of the phosphine donor on the putative niobium nitride results in the oxidation of P(III) to P(V) in **3**. The N−N bond cleavage product **3** indicates a promising route to the functionalization of coordinated N_2 and work is currently underway to examine the reactivity of niobium nitride species stabilized by $[P_2N_2]$ with nucleophilic and electrophilic substrates.

Experimental Section

Unless otherwise stated, all manipulations were performed under an atmosphere of dry oxygen-free nitrogen or argon by means of standard Schlenk or glovebox techniques (Vacuum Atmospheres HE-553-2 glovebox equipped with a MO-40-2H purification system and a −40 °C freezer). Hexanes and toluene were purchased anhydrous from Aldrich and further dried by passage through a tower of alumina and degassed by passage through a tower of Q-5 catalyst under positive pressure of nitrogen.[52] Anhydrous diethyl ether and THF were stored over sieves and distilled from sodium benzophenone ketyl under argon. Nitrogen and argon were dried and deoxygenated by passing the gases through a column containing molecular sieves and MnO. Deuterated benzene and toluene were dried by refluxing over sodium and potassium alloy, d_8-THF was dried over sodium, in a sealed vessel under partial pressure, and then trap-to-trap distilled. They were degassed under 3 freeze−pump−thaw cycles. Unless otherwise stated, all NMR spectra were recorded on a Bruker AVA 400 instrument operating at 400.132 MHz for ^{1}H spectra. Evans method experiments were performed on a Bruker AC 200 instrument operating at 200.132 MHz for ^{1}H spectra. ^{1}H NMR spectra were referenced to residual protons in the deuterated solvent. EPR spectra were obtained on a Bruker ECS 106 spectrometer. UV−vis spectra were recorded with a Hewlett-Packard 8454 UV−visible spectrophotometer and quartz cuvettes with Teflon Kontes valves. Elemental analyses were performed by Mr. P. Borda of this department. Mass spectrometry was performed on a Kratos MS 50 by Mr. M. Lapawa, also of this department. The variable-temperature magnetic susceptibility of powdered samples of **2** and **3** was measured over a temperature range of 2−300 K and at a field of 10 000 G with a Quantum Design (MPMS) SQUID magnetometer. The orbitals obtained by DFT calculations were visualized by using the Molden[53] program.

$([P_2N_2]Nb)_2(\mu\text{-}N_2)$ (2): A mixture of $[P_2N_2]NbCl$ (3.0 g, 4.54 mmol) and KC_8 (0.68 g, 5.00 mmol) was placed in a thick-walled glass reactor fitted with a Teflon Kontes valve. The flask was evacuated and cooled to −196 °C and toluene (100 mL) was added by vacuum transfer; the flask was sealed under an atmosphere of dinitrogen and allowed to warm to 25 °C. After being stirred for 48 h the brown solution was filtered through Celite and solvent removed in vacuo, leaving a brown residue. The solids were washed with hexanes. Yield: 2.5 g (85%). Crystals suitable for X-ray diffraction were obtained by slow evaporation of a saturated toluene solution. ^{1}H NMR (δ, 400 MHz, C_6D_6, ppm): −11.52 ($w_{1/2}$ 768 Hz, 8H, *o*-Ph); 0.82 (88 Hz, 24H, $SiCH_3CH_3'$); 5.44 (216 Hz, 24H, $SiCH_3CH_3'$); 6.60 (120 Hz, 8H, *m*-Ph); 7.67 (32 Hz, 4H, *p*-Ph); 32.39 (2720 Hz, 4H, PC*H*H′). EPR (C_7H_8) g_{iso} = 1.975; $a(^{93}Nb)$ = 108.2 G, 1 Nb; $a(^{31}P)$ = 22.9 G, 2 P. MS (EI) *m*/*z*, (%) 1278, (80) $[M]^+$. μ_{eff}(Evans method) = 2.8 μ_B (per dinuclear molecule). Anal. Calcd for $C_{48}H_{84}N_6Nb_2P_4Si_8$: C, 45.05; H, 6.62; N, 6.57. Found: C, 44.86; H, 6.47; N, 4.13. (Formation of stable niobium nitrides during microanalysis cause consistently low observed values for N.)

$[P_2N_2]Nb(\mu\text{-}N)Nb[PN_3]$ (3): $([P_2N_2]Nb)_2(\mu\text{-}N_2)$ (1.00 g, 0.782 mmol) was dissolved in toluene (50 mL) and placed in a thick-walled glass reactor fitted with a Teflon Kontes valve. The solution was heated to 110 °C for 24 h. The resulting deep blue solution was cooled and filtered through Celite, and the solvent was removed in vacuo to obtain a dark blue solid. Recrystallization from a saturated hexanes solution cooled to −40 °C produced a crop of dark blue crystals. Yield: 0.74 g (74%). MS (EI) *m*/*z*, (%) 639, (80) $[M]^+$. μ_{eff}(Evans method) = 2.7 μ_B (per dinuclear molecule). Anal. Calcd for $C_{48}H_{84}N_6Nb_2P_4Si_8$: C, 45.05; H, 6.62; N, 6.57. Found: C, 44.95; H, 6.57; N, 5.23.

$[P_2N_2]Nb(\eta^2\text{-}HCCPh)$ (4): $([P_2N_2]Nb)_2(\mu\text{-}N_2)$ (1.00 g, 0.782 mmol) was dissolved in toluene (50 mL) and phenylacetylene (160 mg, 1.564 mmol) was added slowly to the stirred brown solution. After 1 h the solution turned dark orange. The reaction was stirred for a further 11 h and filtered and solvents were removed in vacuo to yield a dark orange-brown solid. Yield: 1.00 g (88%). Large dark red crystals were obtained by slow evaporation of a saturated toluene solution. EPR (C_7H_8) g_{iso} = 1.985; $a(^{93}Nb)$ = 108.4 G, 1 Nb; $a(^{31}P)$ = 21.6 G, 2 P. MS (EI) *m*/*z*, (%) 727, (100) $[M]^+$. μ_{eff}(Evans method) = 1.4 μ_B. Anal. Calcd for $C_{32}H_{48}N_2NbP_2Si_4$: C, 52.80; H, 6.65; N, 3.85. Found: C, 52.85; H, 6.85; N, 3.81.

Reaction of 2 with $PbCl_2$. $PbCl_2$ (70 mg, 0.25 mmol) was added to a brown solution of **2** (300 mg, 0.23 mmol) in toluene (30 mL) and the mixture was stirred for 12 h. The resulting green solution was filtered through Celite and toluene was removed in vacuo. NMR and mass spectral data were identical with those for **1**.

Reaction of 2 with $Me_3N{\cdot}HCl$. $Me_3N{\cdot}HCl$ (45 mg, 0.47 mmol) was added to a brown solution of **2** (300 mg, 0.23 mmol) in toluene (30 mL) and the mixture was stirred for 12 h. The resulting green solution was filtered through Celite and toluene was removed in vacuo. NMR and mass spectral data indicate the product to be **1**.

Hydrazine Analysis. Analysis for hydrazine was performed according to published procedure.[54]

X-ray Crystallographic Analyses of 2, 3, and 4. In all cases, suitable crystals were selected and mounted on a glass fiber with use of Paratone-N oil and frozen to −100 °C. All measurements were made on a Rigaku/ADSC CCD area detector with graphite monochromated Mo Kα radiation. Crystallographic data appear in Table 1. In each case the data were processed[55] and corrected for Lorentz and polarization effects and absorption. Neutral atom scattering factors for all non-hydrogen atoms were taken from the *International Tables for X-ray Crystallography*.[56,57] All structures were solved by direct methods[58] and expanded by using Fourier techniques.[59] All non-hydrogen atoms were refined anisotropically. Hydrogen atoms were included but not refined. Hydrogen atoms were fixed in calculated positions with C−H = 0.98 Å.

(52) Pangborn, A. B.; Giardello, M. A.; Grubbs, R. H.; Rosen, R. K.; Timmers, F. J. *Organometallics* **1996**, *15*, 1518.
(53) Schaftenaar, G. *Molden*, 3.5 ed.; CAOS/CAMM Center, University of Nijmegen: Nijmegen, The Netherlands, 1991.
(54) Watt, G. W.; Chrisp, J. D. *Anal. Chem.* **1952**, *24*, 2006.
(55) *teXsan*, Crystal Structure Analysis Package; Molecular Structure Corp.: The Woodlands, TX, 1995.
(56) *International Tables for X-ray Crystallography*; Kluwer Academic: Boston, MA, 1992; Vol. C, pp 200−206.
(57) *International Tables for X-ray Crystallography*; Kynoch Press: Birmingham, U.K. (present distributer Kluwer Academic: Boston, MA), 1974; Vol. IV, pp 99−102.
(58) Altomare, A.; Burla, M. C.; Cammali, G.; Cascarano, M.; Giacovazzo, C.; Guagliardi, A.; Moliterni, A. G. G.; Polidori, G.; Spagna, A. *SIR97*: a new tool for crystal structure determination and refinement, 1999.
(59) Beurskens, P. T.; Admiraal, G.; Beurskens, G.; Bosman, W. P.; de Gelder, R.; Israel, R.; Smits, J. M. M. *DIRDIF94*; The DIRDIF-94 program system, Technical Report of the Crystallography Laboratory; University of Nijmegen: Nijmegen, The Netherlands, 1994.

Acknowledgment. We gratefully acknowledge Professor Robert C. Thompson and Victor Sanchez (UBC) and Professor Natia L. Frank (University of Washington) for help in measurement of the variable-temperature magnetic susceptibilities of **2** and **3** and for stimulating discussions on the subject of magnetism. Barry Liboiron is thanked for assistance with EPR spectroscopy. We thank both the NSERC of Canada and the Petroleum Research Fund, administered by the American Chemical Society, for funding in the form of research grants.

Supporting Information Available: Complete crystallographic data (CIF) for complexes **2**, **3**, and **4**; density functional theory calculation results for model complex **2A** (PDF). This material is available free of charge via the Internet at http://pubs.acs.org.

JA025997F